Applied Catalysis B: Environmental 150–151 (2014) 421–431

Contents lists available at ScienceDirect

Applied Catalysis B: Environmental

journal homepage: www.elsevier.com/locate/apcatb

Silica-poly(styrenesulphonic acid) nanocomposites for the catalytic dehydration of xylose to furfural

I. Sádaba [1], M. Ojeda [2], R. Mariscal, M. López Granados *

Instituto de Catálisis y Petrolequímica (CSIC), C/ Marie Curie 2, Campus de Cantoblanco, 28049 Madrid, Spain

ARTICLE INFO

Article history:
Received 27 October 2013
Received in revised form 5 December 2013
Accepted 13 December 2013
Available online 22 December 2013

Keywords:
Xylose
Furfural
Sol–gel
Poly(styrene sulphonic acid)
Acid catalyst

ABSTRACT

This investigation reports on the catalytic properties and hydrothermal stability of hybrid organic–inorganic nanocomposites based on aminopropyl-functionalised SiO_2 and poly(styrenesulphonic acid) (PSSA). The nanocomposites were characterised by chemical analysis, thermogravimetric analysis (TGA), N_2 adsorption–desorption isotherms, transmission electron microscopy (TEM), as well as Raman, Diffuse Reflectance Infrared Fourier Transform (DRIFT), X-ray Photoelectron (XPS) and ^1H and ^{13}C solid Magic Angle Spinning-Nuclear Magnetic Resonance (MAS-NMR) spectroscopies. The results have proved that the presence of amino-functionalised silica results in stabilisation of the polymer molecules within the particle network of SiO_2. The polymer is anchored to the silica matrix via electrostatic interactions between the sulphonic groups of the polymer molecules and the amino-functions present in the silica. These nanocomposites exhibited promising catalytic activity in xylose dehydration to furfural (at 443 K and after 5 h, ca. 90% xylose conversion, 65% furfural selectivity). When reused for several cycles, deactivation during the first run was observed due to polymer leaching. In successive runs catalytic properties remain stable.

1. Introduction

Furfural is considered a platform molecule that can be transformed into a variety of valuable bio-based chemicals and biofuels [1,2]. Furfural is one of the compounds of the "top 10 + 4" revised list of bio-based product opportunities from carbohydrates [3]. Furfural is obtained from xylose by stepwise dehydration catalysed by acids. These consecutive steps involve a complex mechanism, and several side reactions occur simultaneously (Scheme 1) [1,4]. Industrially, xylose dehydration is conducted using an aqueous solution of a mineral acid (e.g., H_2SO_4) as catalyst [5]. A desirable and greener alternative is to develop reusable catalysts that can minimise waste effluents. One possible approach consists in the use of solid catalysts that can be easily recovered after the reaction and reused subsequently. Many examples of solid catalysts can be found in the recent literature, including zeolites, metal oxides, functionalised silica and commercial sulphonic resins [6–28]. Nevertheless, the main disadvantages of using solid catalyst are: (i) poor stability in the reaction medium because of the presence of highly polar solvents (typically H_2O), and (ii), the deposition of heavy compounds over the active sites, resulting in the catalyst deactivation by fouling and/or poisoning [15,29].

We have previously reported the use of a water-soluble catalyst consisting of poly(styrenesulphonic acid) (PSSA) in xylose dehydration to furfural. It did not experience poisoning or fouling of the active sites by coke deposition, which eliminated the calcination step typically required to regenerate the spent solid [30]. In addition, this polymer was stable and did not present leaching or any other deactivation process driven by the severe hydrothermal reaction conditions. The polymer could be recycled without loss of catalytic activity and separated from the reaction medium using an ultrafiltration process. The utilisation of ultrafiltration for reusing other soluble sulphonic polymer applied to other reactions of interest in biomass valorisation has been reported elsewhere [31].

The polymer ultrafiltration procedure is laborious, it requires special equipment and it takes longer operational time than more conventional procedures, such as filtration or centrifugation; this make the latter separation techniques more preferred options. We report here the results obtained with an inorganic–organic hybrid prepared by the incorporation of the PSSA in a silica matrix. In this way the resulting solid SiO_2–PSSA nanocomposite can be separated from the reaction mixture by conventional procedures. Silica was chosen as a support because of its relative inertness under the reaction conditions of the xylose dehydration. Besides its preparation and characterisation is well documented.

* Corresponding author. Tel.: +34 915854937; fax: +34 915854760.
E-mail address: mlgranados@icp.csic.es (M.L. Granados).
[1] Present address: Haldor Topsøe A/S, Nymøllevej 55, 2800 Kgs. Lyngby, Denmark.
[2] Present address: Conversion Technology Centre, BP Chemicals Ltd, Saltend, Hull HU12 8DS, United Kingdom.

0926-3373/$ – see front matter © 2013 Elsevier B.V. All rights reserved.
http://dx.doi.org/10.1016/j.apcatb.2013.12.025

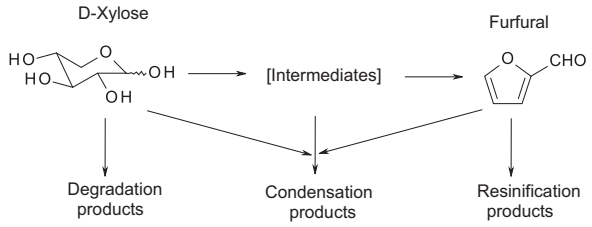

Scheme 1. Simplified overview of the mechanism of D-xylose dehydration to furfural.

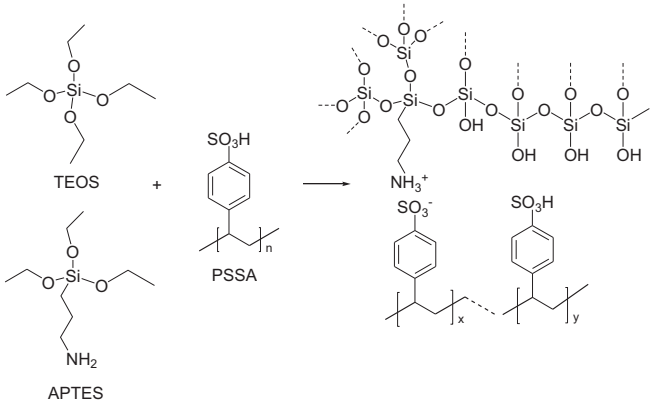

Scheme 2. Preparation of the SiO_2–PSSA catalyst in the presence of APTES.

Several methods have been described for the synthesis of polymer–silica nanocomposites in which strong polymer–silica interactions are formed either via the formation of covalent bonds or via electrostatic interactions [32–34]. These methods result in the fixation of the polymer on the silica surface. A very frequent approach is using in situ polymerisation routes: the monomer is subjected to polymerisation in the presence of the inorganic solid, which is previously formed [35–41]. However a different approach has been selected by us, the anchoring of previously formed PSSA macromolecules. This is more interesting from an environmental point of view because PSSA can be potentially prepared from polystyrene waste [42,43] and therefore this approach paves the way to the reclamation of waste polystyrene as acid catalyst.

Our strategy involves the use of ionic interactions for anchoring the polyelectrolyte macromolecule on the silica surface. Chujo et al. have reported on a synthetic route in which a PSSA polymer with a low sulphonation degree is retained on an amino-functionalised SiO_2 by electrostatic interactions between the sulphonic group of PSSA and the amino groups of the silica [44]. They used sol–gel routes and silica precursors like tetramethoxysilane (TMOS) and 3-aminopropyl trimethoxysilane (APTMOS). The hydrolysis and condensation of these precursors were achieved by the presence of HCl (acid catalyst) and PSSA.

We have used a modification of this synthetic route, no HCl was incorporated and the sulphonic groups of PSSA act as the acid sites for catalysing the hydrolysis and condensation of the silica precursors. Tetraethylorthosilicate (TEOS) and 3-aminopropyltriethoxysilane (APTES) were chosen as SiO_2 precursors which generate environmentally friendly ethanol after hydrolysis, avoiding the presence of methanol in the medium. Moreover we have used a PSSA polymer with a high sulphonation degree to get larger loading of sulphonic sites. The formation of silica nanoparticles through sol–gel route provides high surface area to the final solid. A summary of this protocol is shown in Scheme 2.

Particularly we have explored the effect of incorporation of APTES on the following properties of nanocomposite: formation of electrostatic interactions between sulphonic and amine groups, the hydrothermal stability of the nanocomposite, the leaching of the polymer and the catalytic stability. To achieve such information we have basically studied the incorporation during the synthesis of different amount of APTES with respect to PSSA (no APTES), a minute amount of APTES (mol APTES/TEOS = 0.001) and a larger concentration of APTES (mol APTES/TEOS = 0.5). The rest of variable of synthesis; for example temperature of synthesis, mol H_2O/Si used during the synthesis, type of solvent, etc.; were kept constant.

2. Experimental

2.1. Synthesis of the nanocomposites

First, the required amounts of an aqueous solution of PSSA (Sigma–Aldrich, 18 wt.% in water), tetraethylorthosilicate (TEOS, Sigma–Aldrich, 99%) and 3-aminopropyltriethoxysilane (APTES, Fluka, 96%) were introduced in a round-bottom flask. A reflux condenser was connected, and the flask was immersed in an oil bath at 373 K with magnetic stirring. After 2 h, the formation of a nearly solid gel was observed, and the agitation was terminated. The reactor was maintained under reflux for 17 h, and the solid was filtered thereafter. To remove the residual polymer not retained by the SiO_2 particles, the collected solid was washed with H_2O (ca. 200 mL) under stirring, filtered again and washed until neutral pH. Next, the collected solid was dried at 383 K overnight. Similarly, a blank silica catalyst, which is referred to as Si-5, was synthesised following the same method described above, but using H_2SO_4 instead of PSSA. For the synthesis of Si-5, the amount of H_2SO_4 used equals the amount of sulphonic groups (molar basis) incorporated by the addition of PSSA in the synthesis of the Si-PSSA-5 nanocomposites family

The catalysts are hereafter named as Si-PSSA-*X*-*Y*, where *X* represents the nominal Si/S atomic ratio (different polymer loading), and *Y* indicates the nominal APTES/TEOS ratio (different proportions of amino groups). When *Y* is 0, the number is omitted in the nomenclature. We have explored two different polymer loadings (Si/S = 5 and 12) and two TEOS/APTEOS ratios (0.001 and 0.1) in order to achieve a high polymer loading. It is important to note that when the amount of APTES is notably high, an ammonium sulphonate polysalt can be formed due to the interaction between the different functional groups [43] so we restricted to APTES/APES ratios < 1.

2.2. Characterisation of the nanocomposites

The Si/S atomic ratio of the samples was determined by total-reflection X-ray fluorescence (TXRF) using an Atomika 8030C TXRF spectrometer (Cameca, Germany) equipped with a 3 kW Mo/W dual target X-ray tube and a W/C double monochromator multilayer. A Si(Li) detector with an active area of 80 mm^2 and a resolution of 150 eV at 5.9 keV (Mn Kα) was used for detection and measurement of the produced X-rays. The Si/S atomic ratio was determined using Si Kα and S Kα emission lines in the XRF spectra after proper calibration with standard samples.

The elemental analysis of the solids to determine the S content was performed on a LECO CHNS-932 analyser. Typically, 1 mg of the nanocomposite was placed in an Ag crucible and combusted at 1333 K under a pure O_2 atmosphere. The CO_2, H_2O and SO_2 gases were quantified by Fourier transform infrared (FT-IR) spectroscopy, while N_2 was determined by differential thermal conductivity.

Thermogravimetric analyses (TGA) of the nanocomposites were performed with a Mettler Toledo TGA/SDTA 851e instrument by heating the samples in synthetic air from room temperature to 773 K at a heating rate of 5 K min^{-1}.

N_2 adsorption–desorption isotherms were recorded at 77 K using a Micromeritics TRISTAR 3000 apparatus. The samples were

degassed at 393 K for 12 h prior to determining the adsorption isotherm. The surface area values were calculated using the Brunauer–Emmett–Teller (BET) equation, and the mean pore diameter values were obtained by applying the Barret–Joyner–Halenda (BJH) method to the adsorption branch.

Diffuse reflectance infrared Fourier transform (DRIFT) spectra were obtained with a Nicolet 5700 spectrometer equipped with a globar source and a high sensitivity Hg–Cd–Te type detector working in the 4000–650 cm^{-1} wavenumber range. The spectra were obtained at a resolution of 4 cm^{-1} with an accumulation of 128 scans. A praying Mantis mirror optical accessory and an in situ chamber (Harrick Scientific Products, NY) were used. The finely ground samples (approximately 50 mg) were placed in this chamber and pretreated under Ar flow (approximately 50 mL min^{-1}) at 413 K for 1 h prior to collecting the infrared spectra at room temperature. The DRIFT spectra of PSSA were recorded by adding a few drops of a commercial aqueous solution of α-Al_2O_3 previously loaded in the in situ DRIFT cup, and H_2O was removed by heating at 413 K.

The Raman spectra were recorded with a Renishaw in Via Raman Microscope spectrometer equipped with a laser beam emitting at 785 nm with 15 mW output power. The photons scattered by the sample were dispersed by a 1200 lines/mm grating monochromator and simultaneously collected on a CCD camera. The collection optic was set at 100× objective. The spectral resolution was 1 cm^{-1}.

Transmission electron micrographs (TEM) were acquired with a 200 kV JEOL JEM-2100F microscope equipped with an energy dispersive X-ray (EDX) spectrometer.

The NMR spectra were recorded in an AV-400-WB Bruker spectrometer equipped with a triple channel probe. Samples were finely ground and dried for several days at 373 K in an oven, and then rapidly transferred to ZrO_2 rotors (4 mm) and capped with Kel-F caps to prevent the polymer hydration. The frequency used was 100.32 MHz, the samples were spun at 10 kHz and the CP-MAS ^1H and ^{13}C spectra were recorded using a spectral width of 35 kHz, excitation pulse for ^1H of 3.4 μs, contact time of 3.5 ms, a relaxation time of 4 s, and with ^1H tppm15 decoupling at 80 kHz. The number of collected scans was 1024 and 256 for the ^{13}C and ^1H spectra, respectively. The ^{13}C chemical shifts are referenced to the adamantane CH_2 signal (29.5 ppm) as a secondary reference relative to the tetramethylsilane (TMS) primary reference.

2.3. Catalytic activity in xylose dehydration

Batch catalytic experiments were performed in a pressure glass tube reactor (15 mL capacity) from Ace Glass, Inc. The reactors were purged with N_2 prior to use. In a typical experiment, 150 mg of D-xylose (Sigma–Aldrich, >99%), 100 mg of catalyst, deionised H_2O (1.5 mL) and toluene (3.5 mL, Sigma–Aldrich, >99.5%) were poured into the reactor. This mixture was heated to 443 K by immersion in a thermostatically controlled oil bath and stirred with a magnetic bar at 1000 rpm. The reaction was terminated by withdrawing the reactor from the oil bath and cooling it down in a cold-water bath. Glucose and octanoic acid were used as internal standards for the analysis of the aqueous and organic solutions, respectively.

Reaction products were quantified with an Agilent 1200 HPLC equipped with a refractive index detector in isocratic mode. D-Xylose and furfural present in the aqueous phase were separated on a Rezex RHM 300 × 7.8 mm ion-exchange column (Phenomenex) using 0.005 M H_2SO_4 as mobile phase. The flow rate was 0.4 mL min^{-1}, and the column temperature was maintained at 328 K. The furfural present in the organic phase was quantified with a C18 column (4.6 × 150 mm, Agilent Zorbax Eclipse). The mobile phase consisted of 80 vol.% methanol in water at 0.5 mL min^{-1} at 313 K.

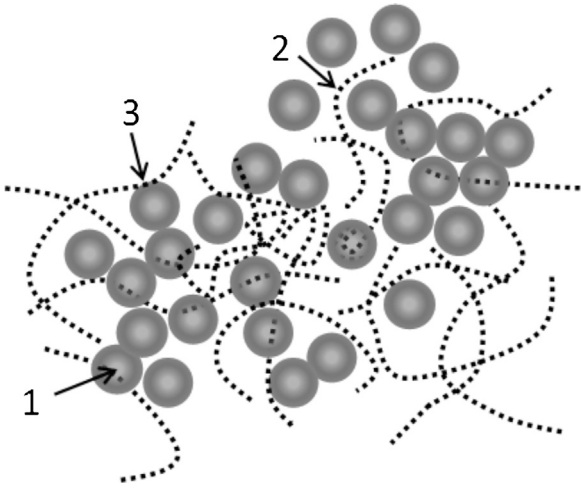

Fig. 1. Possible interactions in the SiO_2–PSSA nanocomposite. The black chains represent molecules of PSSA, while the grey spheres symbolise SiO_2 particles. Situations 1 and 2: physical interactions. Situation 3: chemical electrostatic interaction (see text for explanation).

2.4. Hydrothermal stability of the nanocomposites

To further investigate the stability of the nanocomposites, the samples were subjected to a hydrothermal treatment. For this purpose, approximately 500 mg of the nanocomposite were placed in a pressure glass tube with deionised H_2O (5 mL) at 473 K for 2 h. After the treatment, the solid was recovered by filtration, washed with H_2O until neutral pH, and then dried at 383 K overnight prior to conducting another hydrothermal stability test. The resulting solids were characterised to evaluate the effect of these treatments.

3. Results and discussion

3.1. Preparation and characterisation of the SiO_2–PSSA nanocomposites

Several types of interactions are possible between the polyelectrolyte and the particles of SiO_2 (Fig. 1). The situations represented in Fig. 1 are a simplification (the same polymer molecule may be affected by different interactions and silica particles do not necessarily exhibit a spherical shape), but the picture schematically illustrates the different possible interactions. Because the polymer acts as a hydrolysing agent, silica may grow encapsulating a portion of the PSSA chains (situation 1, Fig. 1). This interaction can firmly immobilise the polymer because part of the macromolecule is embedded within the silica matrix, resulting in the leaching of the polyelectrolyte molecules in the reaction medium being difficult. The polymer can be also embedded within the porous network of SiO_2 nanoparticles (situation 2). Because the polymer is not occluded inside the SiO_2 particles, the polymer may leach easily. A third possibility is that the sulphonic groups can interact electrostatically with certain sites present in the SiO_2 matrix. For example, sulphonic groups can protonate silanol groups, resulting in R–SO_3–H_2O^+–SiO_2 ion pairs that may provide stability to the polymer. When APTES is used in the synthesis of the nanocomposites in addition to TEOS, the aminopropyl groups on the SiO_2 surface can anchor the polymer through electrostatic interactions involving R–SO_3^-–NH_3^+–$(CH_2)_3$–SiO_2 (situation 3, Fig. 1). Such interactions can occur between sulphonic groups from the same or different polymer chains to amino groups located in the same or different SiO_2 particles. It is important to note that this type of electrostatic interaction may also occur in the interior of the particle because the silica growth can occlude the polymer inside

Table 1
Nomenclature and composition of the SiO_2–PSSA nanocomposites.

Catalyst	Nominal Si/S ratio	Experimental Si/S ratio[a]	S content (mmol g_{cat}^{-1})[b]	PSSA (wt.%)[c]
Si-PSSA-12	12	31.8	0.4	6.5 (27.0)
Si-PSSA-5	5	61.2	0.2	3.9 (48.0)
Si-PSSA-5-0.001	5	47.3	0.3	4.9 (48.0)
Si-PSSA-5-0.1	5	7.2	1.5	27.3 (48.0)

[a] Obtained by TXRF.
[b] Calculated from the S content by elemental chemical analysis.
[c] Calculated from S content, assuming that all styrene units are sulphonated (molecular weight 184 g mol^{-1}) relative to the amount of S (atomic weight 32 g mol^{-1}). Values in brackets correspond to the nominal amount of initial polymer loading in the preparation mixture.

the particle. From a practical standpoint, this latter situation is indistinguishable from situation 1. The relative number of these interactions is expected to primarily depends on the relative concentration of polymer, TEOS and APTES. The characterisation work was directed to study the texture and chemical properties of the final nanocomposite, paying specific attention to identify the presence of electrostatic interactions and to find the role of these interactions on the stability of the polymer against leaching at hydrothermal conditions.

Two different variables were explored in the preparation of the nanocomposites: (*i*) two Si/S atomic ratios (5 and 12), and (*ii*) different concentrations of aminopropyl groups. Large Si/S values would result in a low polymer loading and higher amounts of PSSA (low Si/S ratios) would facilitate the leaching of the polymer due to the reduced amount of silica present. These two Si/S ratio were selected as two representative values for a preliminary exploration. A blank silica sample with a Si/S = 5, which is referred to as Si-5, was prepared without PSSA. In this particular experiment, H_2SO_4 was used as the hydrolysing agent. Three APTES/TEOS molar ratios (i.e., N/Si atomic ratio) were selected (APTES/TEOS = 0, 0.001 and 0.1). Higher amounts of APTES may result in the formation of a polysalt by neutralisation of the sulphonic groups with the amino groups, which would largely decrease the number of acid sites in the reaction, thus leading to a decreased activity.

In order to determine the wt.% of C, H, N and S contents, elemental analysis (microanalysis) was performed. Total-reflection X-ray fluorescence (TXRF) was employed to determine the Si/S ratio. Table 1 shows the composition of the catalysts. First, the experimental Si/S ratio is higher than the nominal value in all cases, which indicates that the amount of PSSA incorporated in the nanocomposite is lower than expected and varies depending on the synthesis conditions. By assuming that the degree of sulphonation of the polymer is 100%, the amount of PSSA retained in the solid composite can be calculated from the S content (i.e., all aromatic rings are substituted with sulphonic groups). With the exception of the nanocomposite containing the highest quantity of aminopropyl groups (Si-PSSA-5-0.1), the solids exhibited low PSSA concentrations. For the Si-PSSA-12 sample, the experimental content of PSSA is 6.5 wt.% (vs. theoretical 27 wt.%). For the sample Si-PSSA-5, the experimental content is 3.9 wt.% versus the nominal percentage of PSSA, which is 48 wt.%. From these data, one can infer that in these solids PSSA is retained by the silica matrix by physical interactions only (situations 1 and 2 in Fig. 1). However, this capacity is rather limited for both Si-PSSA-12 and Si-PSSA-5 nanocomposites. The addition of significant quantities of an amino-functionalised silica precursor during the synthesis (catalyst Si-PSSA-5-0.1) results in the incorporation of higher amounts of PSSA (ca. 27%). However, the addition of a small amount of APTEOS during the synthesis (Si-PSSA-5-0.001) did not significantly improve the PSSA loading, and

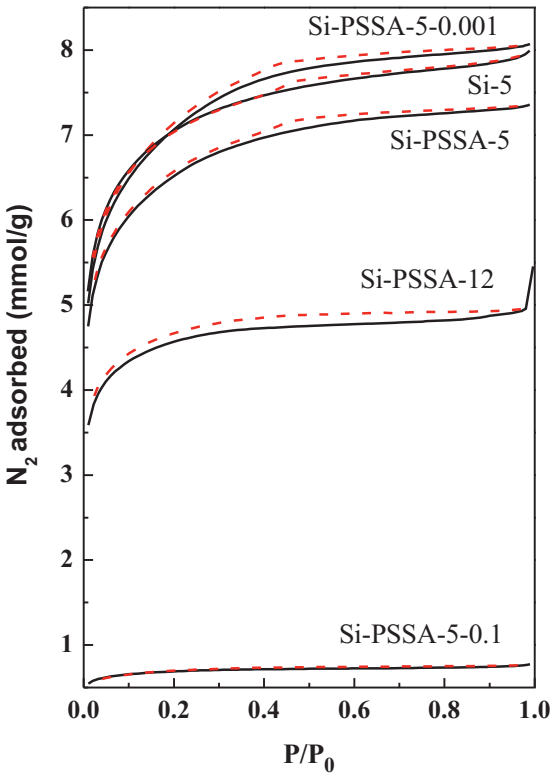

Fig. 2. N_2 adsorption (solid lines) and desorption (dashed lines) isotherms of the SiO_2–PSSA nanocomposites.

less than 5 wt.% of PSSA was incorporated, which is similar to that observed with the Si-PSSA-5 sample.

The textural properties of the solids were studied by N_2 adsorption–desorption isotherms (Fig. 2). The shape of the isotherms could be initially classified as type I, which essentially corresponds to microporous solids [45]. The gentle slope observed at relative pressures above 0.1 is indicative of an activated adsorption due to the presence of micropores. These micropores are filled with polymer molecules and then polymer prevents the rapid filling of the pores, which would require higher pressures to push the N_2 into the micropores. This results in a modification of the effective size of the pores, as it will be shown below. Hysteresis loops are classified as type H4. For sample Si-5 (silica without PSSA), the desorption branch closes at P/P_0 of ca. 0.4 due to the sudden evacuation of the pores, which is an effect known as tensile strength [46]. Nevertheless, this process is not observed in the SiO_2–PSSA nanocomposites, in which the loop does not close. In these cases, a process known as low pressure hysteresis is observed. This phenomenon is often associated with the swelling of an inelastic and non-rigid porous structure during the adsorption cycle [45], which is related here to the lack of rigidity caused by the presence of the polymer inside the pores. The low pressure hysteresis may be also due to irreversible adsorption because the pore size is approximately the width of the adsorbate molecule (N_2) [45]. Nonetheless, this option can be ruled out because the cycle closes abruptly in solid Si-5, indicating that the presence of PSSA in the pores must be responsible for the low-pressure hysteresis phenomenon.

Table 2 summarises the most important textural features of the nanocomposites. In these microporous–mesoporous materials, it is important to note that the use of the BET method to estimate the specific surface area is not realistic because the BET monolayer content in the micropores does not possess the same physical meaning as for the mesopores. The BET surface area of the micropores reflects the retention capacity of micropores and the BET

Table 2
Textural properties of the SiO_2–PSSA nanocomposites.

Catalyst	BET ($m^2\ g^{-1}$)	Micro. *t*-plot ($m^2\ g^{-1}$)	Ext. *t*-plot ($m^2\ g^{-1}$)	Micropores/total[a]
Si-PSSA-12	390	384	6	0.98
Si-5	591	584	7	0.99
Si-PSSA-5	542	538	4	0.99
Si-PSSA-5-0.001	581	576	5	0.99
Si-PSSA-5-0.1	59	58	1	0.98

[a] Ratio between the area of the micropores (*t*-plot) and the total surface area.

surface area of the mesopores estimates its monolayer capacity. For an accurate determination of the BET retention capacity of micropores–mesopores materials, the methodology proposed by Rouquerol et al. was employed [47], and the t-plot method was utilised to discern between the micropores and the external surface due to the mesopores [48].

There are great similarities between the catalysts with the same Si/S atomic ratio = 5 and those with no or small amounts of APTES (Si-5, Si-PSSA-5 and Si-PSSA-5-0.001). These three solids exhibit similar isotherms, comparable values of the BET surface areas and similar mesopore (external) and micropore areas, which indicates a similar texture. Table 2 shows that the solids are essentially microporous because more than 98% of the BET retention capacity corresponds to the filling of micropores. In these three cases, the key factors for controlling the final texture of the silica during synthesis were essentially equal (same concentration of acid groups during the hydrolysis and condensation of the organosilane precursors to form the silica network). In addition, the PSSA loading of these solids is low, preventing a substantial modification of the porous texture with respect to the pure silica sample (Si-5). In the Si-PSSA-12 nanocomposite (synthesised with a lower PSSA concentration and, consequently, at higher pH), the texture and the porous network is different to that of Si-PSSA-5. It is well known that the reaction rates of hydrolysis and condensation of alkylsilanes depends on acid concentration and that the relative differences in these rates configure the final state of the network of silica particle and consequently the N_2 isotherm. In any case, the Si-PSSA-12 solid is still essentially microporous. Interestingly, the presence of silica functionalised with a significant amount of aminopropyl groups (and therefore, a higher percentage of retained PSSA) impacts clearly the texture as well as the porous structure (sample Si-PSSA-5-0.1). In this predominantly microporous nanocomposite, the BET specific area decreases dramatically, which is most likely due to the solids containing more PSSA and the polymer molecules covering the surface of the silica nanoparticles or plugging the pores [49], reducing the BET surface area. This phenomenon will be further investigated in Section 3.3.

Transmission electron microscopy images of three characteristic solids are shown in Fig. 3. As the content of PSSA increases from pure silica (Si-5, Fig. 3a) to 3.9% for Si-PSSA-5 (Fig. 3b) and to 27 wt.% for Si-PSSA-5-0.1, Fig. 3c, the morphology of the solids becomes more compact and loses the appearance of nanoparticle aggregation of SiO_2 that is clearly visible in the Si-5 sample. This effect is more obvious in the Si-PSSA-5-0.1 sample, in which the polymer seems to cover the external surface of the aggregate. This fact is in agreement with the conclusions derived from the N_2 isotherms. The Si/S ratio determined by EDX analysis (6.6) is in agreement with that of TXRF analysis (7.2, see Table 1).

Fig. 4 displays the DRIFT spectra (4000–1100 cm^{-1} region) for selected catalysts after heating at 413 K. Table 3 summarises the primary bands that will be discussed along with their assignments. The Si-5 sample exhibits the typical O—H bands associated to isolated OH silanol on the SiO_2 surface, as well as to silanols H-bonded to other surface OH groups and to surface H_2O molecules [50,51].

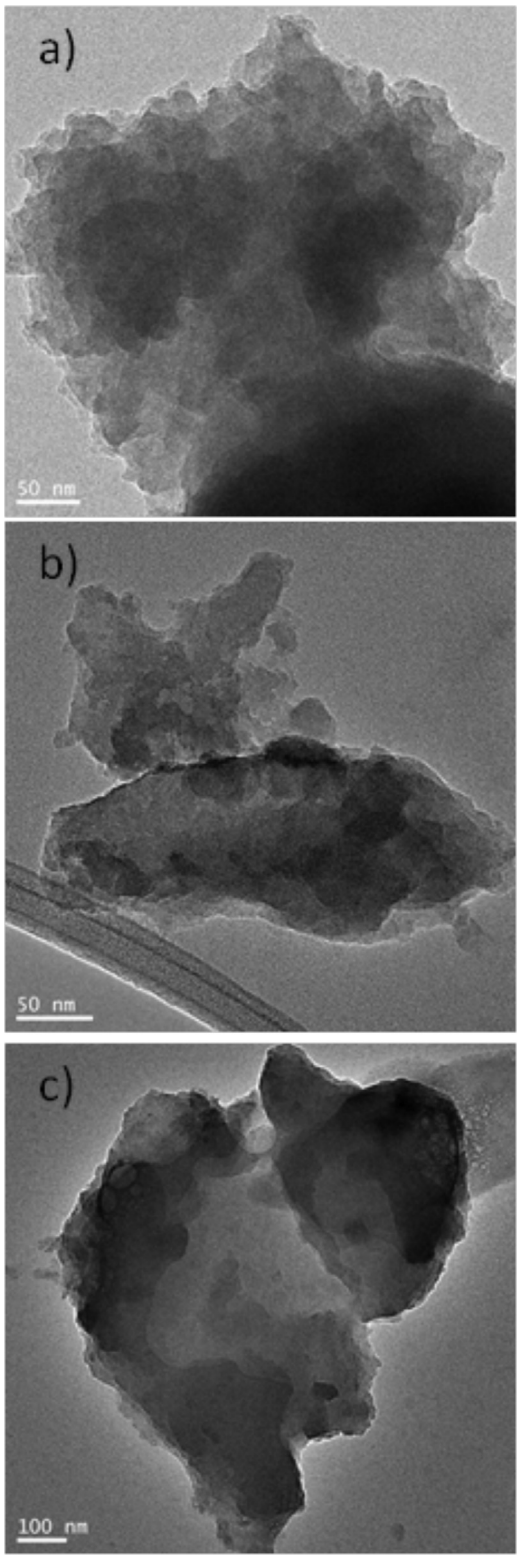

Fig. 3. TEM micrographs of selected nanocomposites: Si-5 (a), Si-PSSA-5 (b), and Si-PSSA-5-0.1 (c).

The rest of the bands observed in the Si-5 spectrum correspond to C—H groups from ethoxy moieties [51] that were not hydrolysed during the synthesis, as well as to lattice Si—O—Si vibration of SiO_2. The Si-PSSA-5-0.001 solid displays a DRIFT spectrum that is notably different from that obtained with the Si-5 sample. The bands from the ethoxy groups are absent (indicating that hydrolysis

Table 3
Assignments of DRIFT bands observed for the SiO_2–PSSA nanocomposites.

Si-5	Si-PSSA-5-0.001	Si-PSSA-5-0.1	PSSA	Assignment
3731	3731			ν(O—H) in isolated silanol
3678	3678			ν(O—H) in H-bonded vicinal silanol
3530	3530			ν(O—H) in silanol H-bonded to water
		3256		ν_{as}(N—H) in R-NH_3^+
		3162		ν_s(N—H) in R-NH_3^+
		3060	3060	ν(C—H) in aromatic ring
		3023	3023	ν(C—H) in aromatic ring
2980				ν_{as}(C—H) in CH_3 (ethoxy group)
2930				ν_{as}(C—H) in CH_2 (ethoxy group)
2910				ν_s(C—H) in CH_3 (ethoxy group)
	2928	2928	2923	ν_{as}(C—H) in CH_2 (polymer backbone)
			2853	ν_s(C—H) in CH (polymer backbone)
		1624		δ_{as}(N—H) in R-NH_3^+
	1595	1595	1595	ν(C—C) in aromatic ring
		1513		δ_s(N—H) in R-NH_3^+
	1493	1493	1493	ν(C—C) in aromatic ring
	1450	1450	1450	ν(C—C) in aromatic ring and δ(C—H) in CH_2 (polymer backbone)
	1415	1415	1415	w(C—H) and/or t(C—H) in CH_2 (polymer backbone)
	1355	1355		ν_{as} O=S=O in SO_3H
1338	1320	1260		ν_{as} (Si—O—Si) in SiO_2

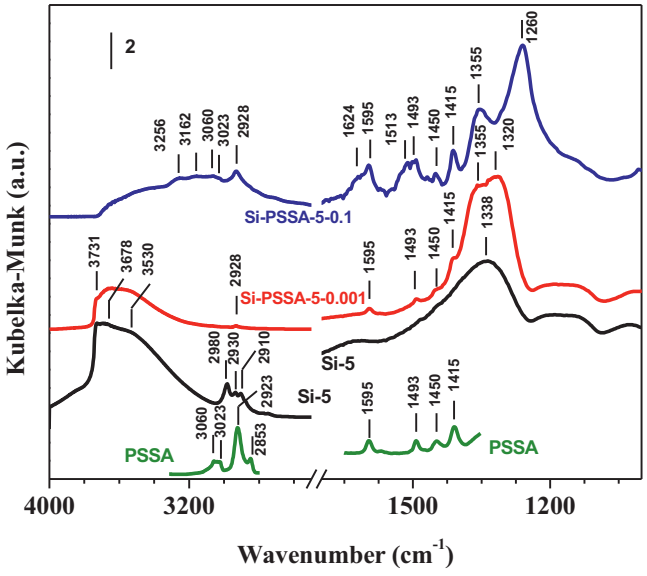

Fig. 4. DRIFT spectra of selected nanocomposites after heating at 413 K under N_2 flow.

of TEOS was complete). The weak band at 2928 cm^{-1} corresponds to C—H vibrations from the polymer retained by the silica matrix. The three weak bands between 1600 and 1450 cm^{-1} arise from C—C and C—H vibrations of the PSSA retained by the silica matrix (see the spectrum of the PSSA polymer included in Fig. 4 for comparison purposes). The unambiguous assignment of a fourth weak band at 1415 cm^{-1} remains elusive, even though it must clearly arise from the polymer. This band is tentatively assigned to C—H deformation in CH_2 units: scissoring (δ), wagging (w) and twisting (t). The same four bands at similar positions have been detected in silica functionalised with 4-ethyl-benzene sulphonic groups [52]. The shoulder band at 1355 cm^{-1} is assigned to the asymmetric stretching vibration of the O=S=O bond in sulphonic groups [53]. Finally, there is a shift in the Si—O—Si band to 1320 cm^{-1} with respect to that in Si-5 (1338 cm^{-1}). The spectra of the Si-PSSA-5-0.1 sample exhibits the same bands assigned to the sulphonic polymer that have been observed in the Si-PSSA-5-0.001 solid. In this case, the bands are more intense, as the polymer loading is now higher. Additional bands at 3060 and 3023 cm^{-1} arising from vibrations of the C—H bonds in the polymer aromatic rings become noticeable. Remarkably, four new IR features are now visible at 3256, 3162, 1624 and 1513 cm^{-1}. The first two correspond to symmetric and asymmetric stretching vibrations of the protonated amine group (R-NH_3^+). These amine bands are now visible because amine loading is higher than in the previous sample. Apparently, the free amine or hydrogen bonded amine, either to sulphonic groups or to silanol groups, are not present, as it would be evidenced by vibrations at significantly different wavenumbers [54]. Similarly, the bands at 1624 and 1513 cm^{-1} are assigned to asymmetric and symmetric N—H bending vibrations in the R-NH_3^+ groups (free and H-bonded amines exhibit these bending bands at substantially different wavenumbers) [54]. Finally, the band pattern from the silanol groups is modified, which is most likely due to the perturbation of the OH groups by the sulphonic groups either through the formation of H-bonds or even by protonation.

The DRIFT data discussed above demonstrate that the amine groups of former APTES groups are protonated by sulphonic groups via an acid–base reaction resulting in the formation of strong electrostatic interactions between the polymer and the SiO_2 surface (Scheme 2). This interaction leads to the stabilisation of the polymer in the silica matrix and explains the elevated polymer loading in this sample. Protonation of amino groups by acid silanols can be discarded. It has been well-documented that protonation by silanol is driven by the presence of H_2O molecules on the surface of the APTES functionalised silica, but this protonation is reversed by H_2O removal either by outgassing or heating above 373 K [55,56]. In addition, H_2O removal would result in the shifting of the amine bands to wavenumbers corresponding to H-bonded amine vibrations. The position of the amine bands in our sample does not change during heating under a N_2 flow (Supplementary Information). Therefore, in the samples studied, the DRIFT amine bands demonstrate that the protonation of the amine groups are driven by sulphonic groups and not by silanol groups. It is important to note that most of the amine groups are protonated, as evidenced by the fact that the bands associated with free or H-bonded amines are not observed. This indicates that all amine groups are involved in the stabilisation of the polymer via electrostatic interactions (acid–base interaction).

Raman spectra of sample Si-PSSA-5-0.1 (recorded at 298 K) after heating in air flow for 1 h at different temperatures were also recorded (see supporting information section, Figure S1). This technique provides unique information for the polymer PSSA

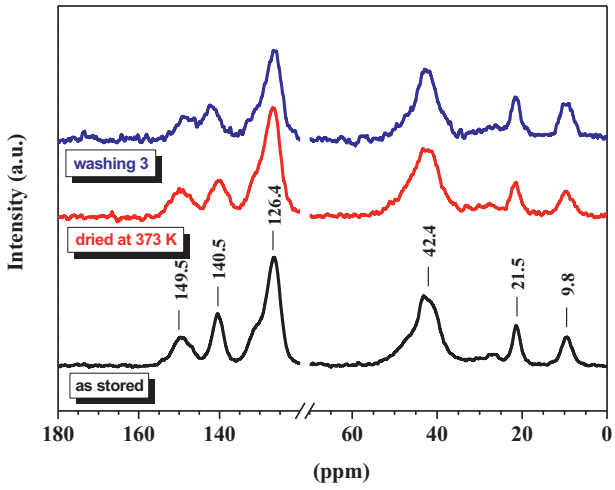

Fig. 5. ^{13}C CP-MAS NMR spectra of the Si-PSSA-5-0.1 fresh sample stored under atmospheric air, after heating at 373 K in air, and after washing with H_2O at 473 K.

because SiO_2 does not exhibit intense Raman bands in this region. Although there is controversy regarding the identification of some of the Raman bands [57–61] (see discussion in support information section), Raman data provides additional support to the hypothesis that sulphonate groups is primarily due to the electrostatic interaction between the amine and the sulphonic group and not to the acid dissociation driven by the presence of H_2O.

Fig. 5 shows the ^{13}C CP-MAS NMR spectra of the Si-PSSA-5-0.1 fresh sample stored under atmospheric air and after heating in air at 373 K. The spectrum labelled as washing 3 will be discussed later. Four signals from the polymer are clearly identified at 42.4 (nonaromatic CH and CH_2 carbons), 126.4 (aromatic C atoms at ortho and meta positions of the sulphonic group C), 140.5 (aromatic C atom bearing the sulphonic group) and 149.5 ppm (C aromatic atom in the para position with respect to the sulphonic group carbon) [30]. Two additional peaks corresponding to the carbon atoms of the aminopropyl groups at 9.8 ppm from Cα and at 21.5 ppm from Cβ are also observed. The signal from Cγ should be detected at approximately 45–50 ppm, but is overshadowed by the peak at 42.4 ppm from the polymer. It is important to note that the Cα and Cβ of the propyl group are sensitive to protonation, especially Cγ The position of these C atoms in the unprotonated amine are shifted approximately 2 and 5 ppm to lower shieldings, respectively, compared to that in Fig. 5. The position of these peaks corresponds to protonated amine groups ($R\text{-}NH_3^+$) [55,56,62]. As explained in the discussion of the DRIFT spectra, the protonation can arise from sulphonic groups or from acidic silanols. However, in the last case, protonation would take place only in the presence of H_2O, and the amine groups would lose the proton under H_2O removal because of the heating treatment conducted at 373 K [55,56]. Therefore, the NMR results agree with the conclusions derived from DRIFT and Raman spectroscopy regarding the formation of an ionic bond between the amine and sulphonic groups.

3.2. Catalytic dehydration of xylose to furfural

The nanocomposites were tested in the dehydration of xylose to furfural (Fig. 6). The values for conversion and yield appearing in the figure are those obtained by a simple experiment. The relative standard deviation of the catalytic activity data was determined to be close to 5%. The Si-PSSA-5-0.1 catalyst exhibits the highest activity (87% xylose conversion after 5 h) among the PSSA-based catalysts tested. This is in good agreement with the elevated PSSA content and consequently larger acid content. Amberlyst 70 was also tested and its conversion included in the figure: it can be seen that the Si-PSSA-5-0.1 catalyst present conversion values close to those of Amberlyst 70. It must be taken into account that according the manufacturer, acid loading of the Amberlyst 70 (2.74 mmol H^+ g_{cat}^{-1}) is larger than that of Si-PSSA-5-0.1 catalyst. The latter solid present 1.5 mmol S g_{cat}^{-1}, but the actual acid loading is smaller than that as a large fraction of the sulphonic groups are neutralised because of the interaction with amino groups. The acid sites loading was measured by titration with KOH and was found to be 0.6 mmol H^+ g_{cat}^{-1} (detailed description of the procedure of titration is given in the supporting information section). The rest of the PSSA based catalysts exhibit lower conversions than that of the Si-PSSA-5-0.1 catalyst (55–60% after 5 h of reaction). The pure silica catalyst (Si-5) converted 30% of the xylose after 5 h of reaction (the curve line that has been traced in the figure is just a visual help), which is comparable with the blank experiment without a catalyst. Therefore, the active sites are due to the sulphonated polymer. The furfural yield obtained with the Si-PSSA-5-0.1 at large conversion values (55%) is comparable to the values obtained with Amberlyst 70 and to those values reported in literature at similar reaction conditions (50–70%) [63–66]. In addition, when comparing the activity data of the Si-PSSA-5-0.1 nanocomposite with that shown by the non anchored polymer [30] normalised by the S content, both catalysts show similar values, 4.2×10^{-4} and 3.8×10^{-4} $mmol_F$ mol S^{-1} s^{-1}, respectively, after 60 min of reaction.

Next, the reusability of the catalysts was studied. The nanocomposites were used in three successive catalytic cycles. The reactions were performed under the same conditions as in the previous case. After 60 min, the catalyst was recovered by centrifugation and washed with water and methanol to remove the reactants and products retained by the solid (this step is necessary to prevent errors in the activity measurement in subsequent cycles). Fig. 7 shows xylose conversion and furfural yield in three successive reaction runs with different Si-PSSA catalysts. The nanocomposite with the highest initial conversion and yields, Si-PSSA-5-0.1, displays the largest initial conversion and yields values as also possesses the highest polymer loading. Although it deactivates during the first run, the catalytic properties remain quite stable for the second and third run with conversion and yield values (ca. 30% and 20%, respectively) significantly above the value obtained for the rest of the catalysts reported in the figure (ca. 15 and 10%, respectively). Experiments without catalyst conducted in the same reactors and with the same reaction conditions after 60 min of reaction but at 453 K (10 K higher than our experiments), gave a conversion of 10% and a yield of 5%, well below the values of run 2 and 3 of Si-PSSA-5-0.1 catalyst. So we can conclude that thermal contribution at 443 K to the activity of Si-PSSA-5-0.1 must be practically negligible.

All the former results demonstrate the importance of incorporating APTES in the synthesis of the nanocomposites to provide larger initial polymer concentration, which is needed to increase the presence of acid sites, and more stability to the catalytic properties. It seems that the presence of amino groups improves the retention of polymer under the hydrothermal conditions of the reaction but it cannot prevent the initial loss of part of the polymer loading. In the next section the study of the hydrothermal stability of the nanocomposite will be described.

3.3. Thermal and hydrothermal stability of the nanocomposites

TGA studies were conducted to assess on the thermal stability of the nanocomposites under air (see supporting information section). The materials are thermally stable up to 550 K, which is a temperature much higher than that frequently used in xylose dehydration reactions (443–473 K).

A thorough study was also accomplished to detect the presence of leaching and homogeneous contribution from the catalyst. The

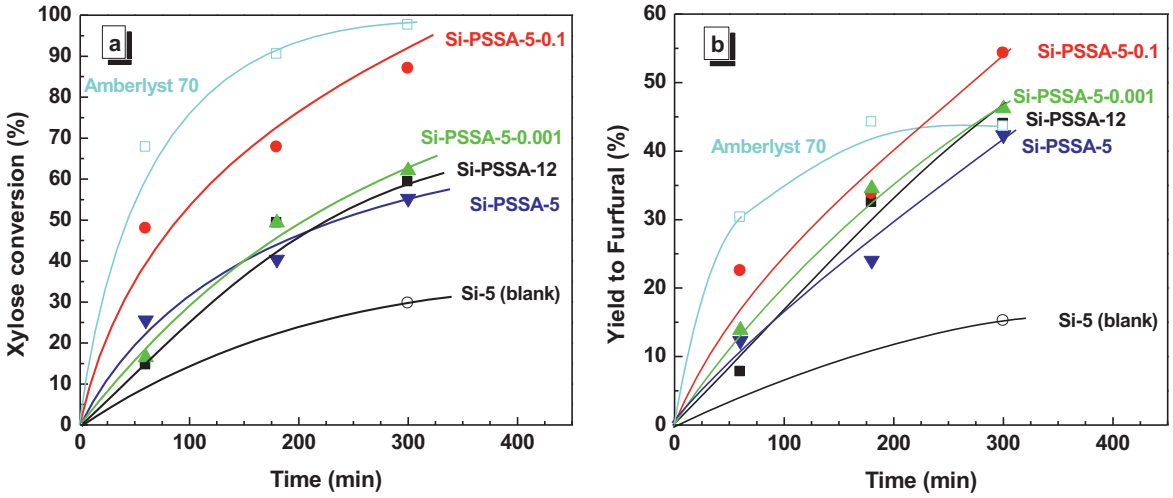

Fig. 6. Catalytic activity of the SiO_2–PSSA nanocomposites. (a) Xylose conversion and (b) furfural yield as a function of reaction time: (●) Si-PSSA-5-0.1, (▲) Si-PSSA-5-0.001, (▼) Si-PSSA-5, (■) Si-PSSA-12, (○) Si-5, (□) Amberlyst 70. Reaction conditions: 0.15 g xylose, substrate/catalyst mass ratio = 1.5, 443 K, 5 mL water–toluene mixture (3:7 volume ratio).

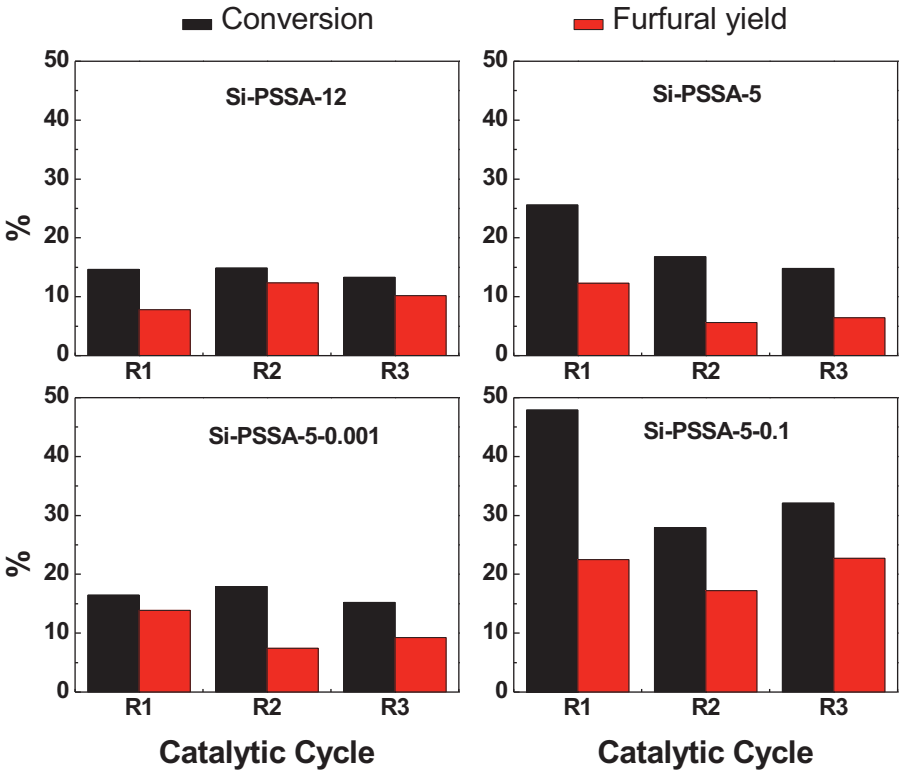

Fig. 7. Recycling of the catalysts for the Si-PSSA series. Reaction conditions: 0.15 g xylose, substrate/catalyst mass ratio = 1.5, 443 K, 5 mL water–toluene mixture (3:7 volume ratio), 60 min.

nanocomposites with a Si/S ratio of 5 were selected for consecutive hydrothermal treatments (washing steps) with H_2O at 473 K. The chemical analyses of the samples containing PSSA and zero or low APTES content show that weakly fixed polyelectrolyte chains not retained by electrostatic interactions are leached (Table 4). For the nanocomposite Si-PSSA-5-0.1 (with the larger APTES loading incorporated to the silica network), a detectable loss of S is also observed during the three washing steps, although in a lesser extension. This result reinforces the importance of using APTES during the synthesis to provide electrostatic interactions that helps to retain the polymer, even when subjected to hydrothermal conditions.

The textural properties of the nanocomposites undergo pronounced modifications after hydrothermal treatments (Fig. 8), leading to a change in the isotherm type from type I to type IV. In addition, H2 hysteresis loops are observed in all cases, except for pure SiO_2, which exhibits an H3-type. The effect depends on the initial amount of PSSA present. For those samples with zero or low PSSA loadings (Si-5, Si-PSSA-5 and Si-PSSA-5-0.001), the surface area decreases with the treatments. This reduction was primarily due to a loss of microporosity (further details can be found in Supplementary Information). The modification of the porous texture is most likely due to two effects. First, the leaching of the polymer

Table 4
Characterisation of the solids after hydrothermal treatment.

Catalyst	Treatment	S content (mmol g_{cat}^{-1})	PSSA content (wt.%)[a]	S_{BET} ($m^2\ g^{-1}$)
Si-5	Fresh	–	–	591
	Washing 1	–	–	119
Si-PSSA-5	Fresh	0.2	3.9	542
	Washing 1	0.1	1.8	275
	Washing 2	0.1	1.1	–
Si-PSSA-5-0.001	Fresh	0.3	4.9	581
	Washing1	0.2	3.0	384
	Washing 2	0.1	2.8	321
Si-PSSA-5-0.1	Fresh	1.5	27.3	59
	Washing 1	1.4	25.7	100
	Washing 2	1.3	23.6	233
	Washing 3	1.4	25.7	247

[a] Calculated from S content, assuming all of the styrene molecules are sulphonated (molecular weight 184 g mol^{-1}) relative to the amount of S (atomic weight 32 g mol^{-1}).

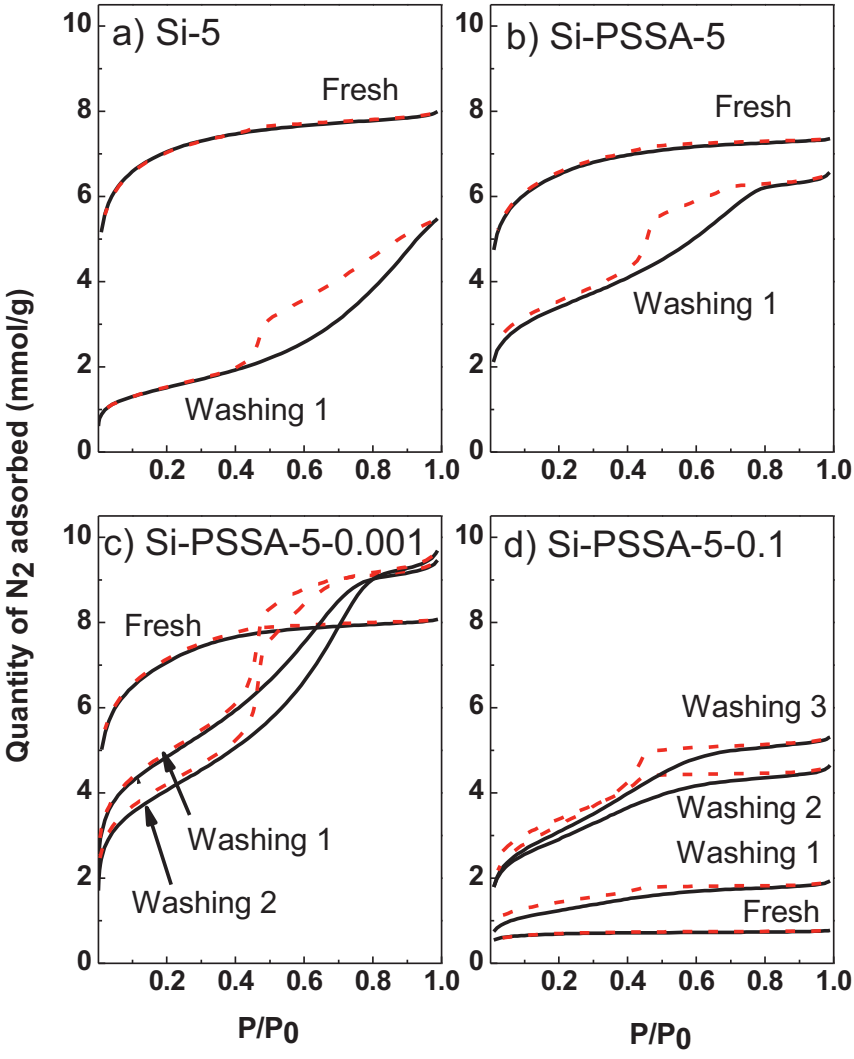

Fig. 8. N_2 adsorption–desorption isotherms of the SiO_2–PSSA nanocomposites after washing treatments.

is favoured by the weak interactions between the polymer and the surface groups (nil or low concentration of amine groups). Second, the high temperatures used for the hydrothermal treatments results in an ageing process involving the additional condensation of silanol groups, which increases the density of the initial gel.

Remarkably, Si-PSSA-5-0.1 suffers an increase in the BET surface area during the washing steps. In this particular case, external mesoporosity is created during the procedure. This surface modification is due to the fact that the fresh Si-PSSA-5-0.1 possesses a notably low surface area because part of the polymer covers the aggregates of particles and blocks the access to the pores. The hydrothermal treatment causes a rearrangement of these compactly conglomerated particles, allowing the formation of interparticle mesoporosity. In fact, it is possible to detect the appearance of pores at approximately 3 nm in the BJH pore size distribution (Figure S3 in supporting information section). In

addition, the TEM study corroborates this hypothesis (see Figure S4 in supporting information section), it reveals a modification in the structure and shows a much looser aggregation of the particles after three cycles of hydrothermal treatments.

For the leaching of the Si-PSSA-5-0.1 nanocomposite, further studies were conducted. XPS analyses verified that no significant changes are detected after the second washing step (see Table S2 of the Supplementary Information). The Raman spectra of the treated nanocomposites do not exhibit considerable differences (see Figure S5 of the Supplementary Information). However, a closer examination of the relative intensities of the bands (see Table S3 of the Supplementary Information) indicated that after hydrothermal treatment, there exists a slight decrease in the intensity of sulphonic groups with respect to the aromatic ring band at 1008 cm^{-1} (for instance, 2.39–2.33 vs. 3.39), which indicates a relative loss of sulphonic groups. Importantly, the loss of S is negligible after the second washing step. All these data are consistent with the previous results.

Finally, the effect of leached species on the catalytic activity was evaluated. We have verified that the Si-PSSA-5-0.1 nanocomposite was recyclable even though some leaching occurs during the first cycle, which was verified by the loss of S in the hydrothermal treatments. The following experiment was conducted to determine whether these leached species were active in the reaction. The as-synthesised catalyst was placed in contact with the reaction medium (H_2O and toluene) for 300 min at 443 K. Next, the catalyst was filtered, and xylose was added to this filtered liquid to conduct the reaction. The xylose conversion after 300 min was 68%, which is much higher than the blank experiment (30%) but also lower than the 87% obtained in the first cycle of the solid catalyst (see Figure S6 of the Supplementary Information for more details). These results indicate that acid species leached during the first cycle contribute to the overall catalytic activity obtained in the first run. Solid Si-PSSA-5-0.1 was subjected to a second extensive hydrothermal treatment for 300 min. The recovered catalyst was employed in another homogeneous contribution test similar to that described above. The activity of the leached species derived from this additional leaching treatment was comparable to the blank experiment (35 vs. 30%). This result indicates that the leaching, and consequently, the contribution of the corresponding lixiviated species to the overall activity were important only in the first cycle and negligible in successive cycles.

In summary, the Si-PSSA-5-0.1 nanocomposite suffers of a limited leaching process during the first hydrothermal contact and a change in the textural structure of the solid resulting in mesoporosity. The composition of the solid remains constant in successive hydrothermal treatment, as shown by chemical analyses, XPS and Raman spectroscopy. The species leached during the first cycle are active in the dehydration of xylose, even though their homogeneous contribution does not represent the total activity of the catalyst. In successive cycles leaching is negligible and so is the contribution to the overall activity of the leached species. A hydrothermal conditioning of the catalyst prior to initiating the catalytic reaction would prevent the leaching of the sulphonic polymer into the reaction medium.

All the previous results demonstrate that the leaching of the polymer is an important cause of deactivation. Additionally, deposition of organic molecules cannot be discarded as a source of deactivation. Heavy products, very likely arising from non-selective side reactions (condensation and resinification products), are prone to be deposited over the silica surface and even partially occluding the pores. Actually by TGA analysis conducted under air on used catalysts (results not shown) evidenced the presence of other features than those arising from the combustion of the polymer. In any case the impact is more limited than that of the leaching as the deactivation does not progress after the second run.

Finally it is important to emphasise two aspects. First, the synthesis route for SiO_2–PSSA nanocomposites here presented does not require in situ polymerisation of sulphonic styrene monomers because it utilises previously formed PSSA. In this investigation commercial PSSA has been used. However, polystyrene can be sulphonated to PSSA and this implies that waste polystyrene previously sulphonated can be also utilised for the synthesis of this nanocomposite. This paves the way to the reclamation of polystyrene as reusable acid catalysts. Second, although these catalysts have been tested for the dehydration of xylose, the nanocomposites could be also applied in other acid-catalysed reactions, especially in important processes in biorefineries.

4. Conclusions

This work represents a preliminary study on the feasibility of the heterogenisation of the sulphonic polymer PSSA for use as catalyst in the reaction of xylose dehydration to furfural. A sol–gel route was selected to form silica–polymer nanocomposites. The characterisation of the solids after hydrothermal treatment demonstrated that the presence of silica functionalised with aminopropyl groups is central to improve the catalytic properties and the stability in terms of minimising the leaching of the polymer. The formation of electrostatic interactions between amino and sulphonic groups explains the better retention of the polymer by the network of silica particles. Further optimisation of variable synthesis is still required to improve the hydrothermal stability of the final nanocomposite, mainly regarding the polymer leaching, and also the furfural yields obtained.

Acknowledgments

This work was funded by the Spanish Ministry of Economy and Competitiveness (Project CTQ2012-38204-C03-01, CARBIOCAT) and the Autonomous Government of Madrid (S2009/ENE-1660, CARDENER-CM partly funded by FSE funds). I.S. wishes to thank the Spanish National Research Council (CSIC) for her contract under the JAE-Predoc programme.

Appendix A. Supplementary data

Supplementary data associated with this article can be found, in the online version, at http://dx.doi.org/10.1016/j.apcatb.2013.12.025.

References

[1] K.J. Zeitsch, The Chemistry and Technology of Furfural and Its Many By-products, Sugar Series, vol. 13, Elsevier, The Netherlands, 2000.
[2] J.P. Lange, E. Van Der Heide, J. Van Buijtenen, R. Price, ChemSusChem 5 (2012) 150–166.
[3] J.J. Bozell, G.R. Petersen, Green Chem. 12 (2010) 539–554.
[4] M.J. Antal, T. Leesomboon, W.S. Mok, Carbohydr. Res. 217 (1991) 71–85.
[5] R. Karinen, K. Vilonen, M. Niemelä, ChemSusChem 4 (2011) 1002–1016.
[6] R. O'Neill, M. Ahmad, L. Vanoye, F. Aiouache, Ind. Eng. Chem. Res. 48 (2009) 4300–4306.
[7] S. Lima, M. Pillinger, A.A. Valente, Catal. Commun. 9 (2008) 2144–2148.
[8] A. Chareonlimkun, V. Champreda, A. Shotipruk, N. Laosiripojana, Bioresour. Technol. 101 (2010) 4179–4186.
[9] A.S. Dias, M. Pillinger, A.A. Valente, Microporous Mesoporous Mater. 94 (2006) 214–225.
[10] A.S. Dias, M. Pillinger, A.A. Valente, J. Catal. 229 (2005) 414–423.
[11] A.S. Dias, M. Pillinger, A.A. Valente, Appl. Catal. A 285 (2005) 126–131.
[12] A.S. Dias, S. Lima, D. Carriazo, V. Rives, M. Pillinger, A.A. Valente, J. Catal. 244 (2006) 230–237.
[13] S. Lima, P. Neves, M.M. Antunes, M. Pillinger, N. Ignatyev, A.A. Valente, Appl. Catal. A 363 (2009) 93–99.
[14] C. Moreau, R. Durand, D. Peyron, J. Duhamet, P. Rivalier, Ind. Crops Prod. 7 (1998) 95–99.
[15] S. Lima, A. Fernandes, M.M. Antunes, M. Pillinger, F. Ribeiro, A.A. Valente, Catal. Lett. 135 (2010) 41–47.

[16] S. Lima, M.M. Antunes, A. Fernandes, M. Pillinger, F. Ribeiro, A.A. Valente, Appl. Catal. A 388 (2010) 141–148.
[17] J. Zhang, J. Zhuang, L. Lin, S. Liu, Z. Zhang, Biomass Bioenergy 39 (2010) 73–77.
[18] A.S. Dias, S. Lima, M. Pillinger, A.A. Valente, Catal. Lett. 114 (2007) 151–160.
[19] Y.C. Kim, H.S. Lee, J. Ind. Eng. Chem. 7 (2001) 424–429.
[20] S.B. Kim, S.J. You, Y.T. Kim, S. Lee, H. Lee, K. Park, E.D. Park, Korean J. Chem. Eng. 28 (2011) 710–716.
[21] X. Shi, Y. Wu, P. Li, H. Yi, M. Yang, G. Wang, Carbohydr. Res. 346 (2011) 480–487.
[22] G.H. Jeong, E.G. Kim, S.B. Kim, E.D. Park, S.W. Kim, Microporous Mesoporous Mater. 144 (2011) 134–139.
[23] I. Agirrezabal-Telleria, A. Larreategui, J. Requies, M.B. Gómez, P.L. Arias, Bioresour. Technol. 102 (2011) 7478–7485.
[24] T. Suzuki, T. Yokoi, R. Otomo, J.N. Kondo, T. Tatsumi, Appl. Catal. A 408 (2011) 117–124.
[25] V. Choudhary, A.B. Pinar, S.I. Sandler, D.G. Vlachos, R.F. Lobo, ACS Catal. 1 (2011) 1724–1728.
[26] E. Lam, J.H. Chong, E. Majid, Y. Liu, S. Hrapovic, A.C.W. Leung, J.H.T. Luong, Carbon 50 (2012) 1033–1043.
[27] I. Agirrezabal-Telleria, J. Requies, M.B. Güemez, P.L. Arias, Green Chem. 14 (2012) 3132–3140.
[28] M.M. Antunes, S. Lima, A. Fernandes, J. Candeias, M. Pillinger, S.M. Rocha, M.F. Ribeiro, A.A. Valente, Catal. Today 195 (2012) 127–135.
[29] I. Sádaba, S. Lima, A.A. Valente, M. López Granados, Carbohydr. Res. 346 (2011) 2785–2791.
[30] M.L. Granados, A.C. Alba-Rubio, I. Sadaba, R. Mariscal, I. Mateos-Aparicio, A. Heras, Green Chem. 13 (2011) 3203–3212.
[31] S. Van De Vyver, J. Thomas, J. Geboers, S. Keyzer, M. Smet, W. Dehaen, P.A. Jacobs, B.F. Sels, Energy Environ. Sci. 4 (2011) 3601–3610.
[32] G. Kickelbick, Prog. Polym. Sci. 28 (2003) 83–114.
[33] H. Zou, S. Wu, J. Shen, Chem. Rev. 108 (2008) 3893–3957.
[34] B.P. Tripathi, V.K. Shahi, Prog. Polym. Sci. 36 (2011) 945–979.
[35] Z. Lei, Y. Li, X. Wei, J. Solid State Chem. 181 (2008) 480–486.
[36] C. Li, J. Yang, P. Wang, J. Liu, Q. Yang, Microporous Mesoporous Mater. 123 (2009) 228–233.
[37] A. Martín, G. Morales, F. Martínez, R. Van Grieken, L. Cao, M. Kruk, J. Mater. Chem. 20 (2010) 8026–8035.
[38] W. Long, C.W. Jones, ACS Catal. 1 (2011) 674–681.
[39] G. Morales, R. van Grieken, A. Martín, F. Martínez, Chem. Eng. J. 161 (2010) 388–396.
[40] J. Jang, H. Park, J. Appl. Polym. Sci. 85 (2002) 2074–2083.
[41] A. Schmid, S.P. Armes, C.A.P. Leite, F. Galembeck, Langmuir 25 (2009) 2486–2494.
[42] W.W. Sulkowski, A. Wolinska, B. Szoltysik, W.M. Bajdur, A. Sulkowska, Polym. Degrad. Stab. 90 (2005) 272–280.
[43] Y. Inagaki, M. Kuromiya, T. Noguchi, H. Watanabe, Langmuir 15 (1999) 4171–4175.
[44] R. Tamaki, Y. Chujo, Chem. Mater. 11 (1999) 1719–1726.
[45] V.K. Shahi, Solid State Ionics 177 (2007) 3395–3404.
[46] D.S. Kim, M.D. Guiver, M.Y. Seo, H.I. Cho, D.H. Kim, J.W. Rhim, G.Y. Moon, S.Y. Nam, Macromol. Res. 15 (2007) 412–417.
[47] K.S.W. Sing, Pure Appl. Chem. 54 (1982) 2201–2218.
[48] J.C. Groen, L.A.A. Peffer, J. Pérez-Ramírez, Microporous Mesoporous Mater. 60 (2003) 1–17.
[49] J. Rouquerol, P. Llewellyn, F. Rouquerol, F.R.-R.J.R.P.L. Llewellyn, N. Seaton, Stud. Surf. Sci. Catal. 160 (2007) 49–56.
[50] B.C. Lippens, J.H. de Boer, J. Catal. 4 (1965) 319–323.
[51] K. Nakanishi, N. Soga, J. Non-Cryst. Solids 108 (1989) 157–162.
[52] G. Orcel, J. Phalippou, L.L. Hench, J. Non-Cryst. Solids 88 (1986) 114–130.
[53] P. Innocenzi, J. Non-Cryst. Solids 316 (2003) 309–319.
[54] A.C. Alba-Rubio, F. Vila, D.M. Alonso, M. Ojeda, R. Mariscal, M. López Granados, Appl. Catal. B 95 (2010) 279–287.
[55] X.D. Fan, C. Geraldine Bazuin, Macromolecules 28 (1995) 8209–8215.
[56] H. Okabayashi, I. Shimizu, E. Nishio, C.J. O'Connor, Colloid. Polym. Sci. 275 (1997) 744–753.
[57] G. Stephen Caravajal, D.E. Leyden, G.R. Quinting, G.E. Maciel, Anal. Chem. 60 (1988) 1776–1786.
[58] C.H. Chiang, N.I. Liu, J.L. Koenig, J. Colloid Interface Sci. 86 (1982) 26–34.
[59] H.G.M. Edwards, D.R. Brown, J.A. Dale, S. Plant, Vib. Spectrosc. 24 (2000) 213–224.
[60] J.M. Alía, H.G.M. Edwards, B.M. Kiernan, Spectrochim. Acta A 60 (2004) 1533–1542.
[61] J.M. Alía, H.G.M. Edwards, B.M. Kiernan, J. Raman Spectrosc. 35 (2004) 111–118.
[62] M. Ristova, L. Pejov, M. Žugić, B. Šoptrajanov, J. Mol. Struct. 482–483 (1999) 647–651.
[63] H.G.M. Edwards, D.R. Brown, J.R. Dale, S. Plant, J. Mol. Struct. 595 (2001) 111–125.
[64] J.E. Sarneski, H.L. Surprenant, F.K. Molen, C.N. Reilley, Anal. Chem. 47 (1975) 2116–2124.
[65] P.A. Russo, S. Lima, V. Rebuttini, M. Pillinger, M.-G. Willinger, N. Pinna, A.A. Valente, RSC Adv. 3 (2013) 2595–2603.
[66] A.S. Dias, S. Lima, M. Pillinger, A.A. Valente (Eds.), Ideas in Chemistry and Molecular Sciences: Advances in Synthetic Chemistry, Wiley-VCH, Weinheim, 2010.